

Journal of Materials Chemistry A

Accepted Manuscript

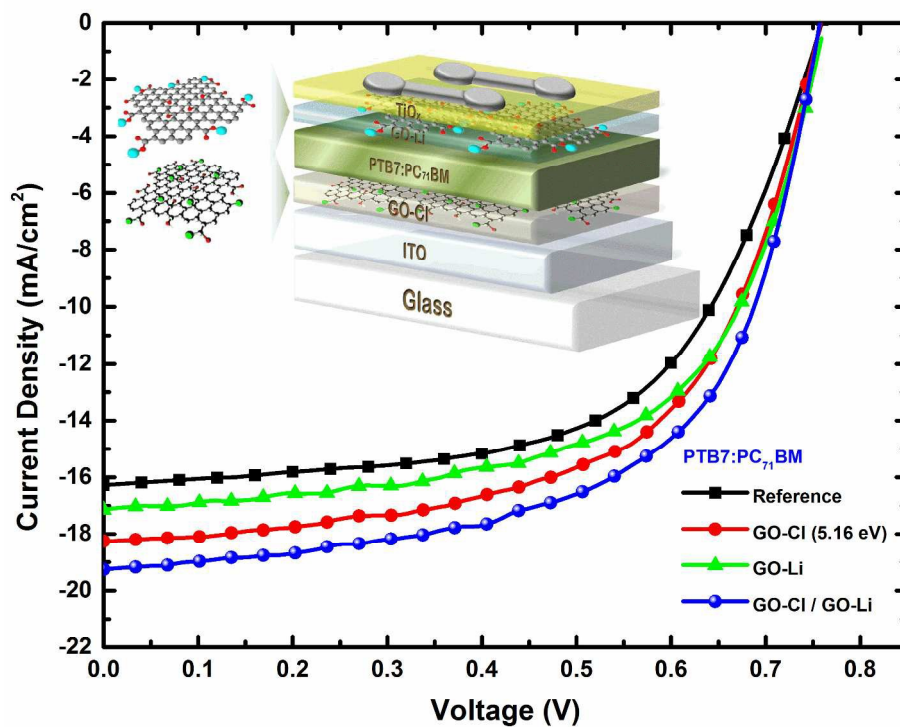


This is an *Accepted Manuscript*, which has been through the Royal Society of Chemistry peer review process and has been accepted for publication.

Accepted Manuscripts are published online shortly after acceptance, before technical editing, formatting and proof reading. Using this free service, authors can make their results available to the community, in citable form, before we publish the edited article. We will replace this *Accepted Manuscript* with the edited and formatted *Advance Article* as soon as it is available.

You can find more information about *Accepted Manuscripts* in the [Information for Authors](#).

Please note that technical editing may introduce minor changes to the text and/or graphics, which may alter content. The journal's standard [Terms & Conditions](#) and the [Ethical guidelines](#) still apply. In no event shall the Royal Society of Chemistry be held responsible for any errors or omissions in this *Accepted Manuscript* or any consequences arising from the use of any information it contains.



271x203mm (300 x 300 DPI)

High efficient organic photovoltaic devices utilizing work-function tuned graphene oxide derivatives as the anode and cathode charge extraction layer

Dimitrios Konios,^{§a} George Kakavelakis,^{§a} Costantinos Petridis,^a Kyriaki Savva,^{a,b} Emmanuel Stratakis,^{a,b} and Emmanuel Kymakis^{*a}

^a Center of Materials Technology and Photonics & Electrical Engineering Department, School of Applied Technology, Technological Educational Institute (TEI) of Crete, Heraklion, 71004 Crete, Greece. Email: kymakis@staff.teicrete.gr; Tel: +30-2810-379895

^b Institute of Electronic Structure and Laser (IESL), Foundation for Research and Technology-Hellas (FORTH), Greece

[§] Authors with equal contribution

Abstract

The effective utilization of work-function (WF) tuned solution processable graphene-based derivatives as both hole and electron transport layers in organic photovoltaic (OPV) devices is demonstrated. The systematic tuning of functionalized graphene oxide (GO) WF took place by either photochlorination for WF increase, or lithium neutralization for WF decrease. In this way, the WF of the photochlorinated GO layer was perfectly matched with the HOMO level of two different polymer donors, enabling excellent hole transport. While the WF of the lithium functionalized GO was perfectly matched with the LUMO level of the fullerene acceptor, enabling excellent electron transport. The utilization of these graphene-based hole and electron transport layers in PTB7:PC₇₁BM active layer devices, led to ~19% enhancement in power conversion efficiency (PCE) compared to the reference graphene free device, resulting in the highest reported PCE for graphene-based buffer layer OPVs of 9.14%. The proposed techniques open new paths towards novel material and interface engineering approaches for a wide range of new applications, including flexible electronics, OPVs, perovskite solar cells, organic light emitting diodes, and photosensors, as well as traditional electronic devices.

Introduction

During the past decade, OPV devices based on the bulk heterojunction (BHJ) blend have attracted great interest due to their potential for low fabrication cost but, more importantly their versatility for large-scale fabrication on flexible substrates.^{1,2,3,4} Despite the numerous studies on OPVs, their power conversion efficiency (PCE) compared to the silicon and other inorganic materials based photovoltaic technologies remains relatively low (~10%).⁵ Aiming to improve the competitiveness of OPVs, extensive research effort has been devoted to the interface engineering of devices and especially to the introduction of charge extracting interlayers between the BHJ layer and the electrodes.^{6,7}

In contrast to inorganic PVs where surface doping is responsible for Ohmic contacts, OPVs require alternative strategies in terms of the interface engineering. The introduction of buffer layers with electron and hole blocking (or transport) properties between the donor:acceptor active layer and the anode and cathode respectively, can effectively reduce recombination and current leakage generated at the photoactive layer-electrode interface and enhance the open circuit voltage (V_{oc}) of the device⁸. A number of hole transporting layer (HTL) materials for OPVs have been used, including transition metal oxides (e.g. MoO_3 , NiO)^{9,10} and self-assembled organic molecules^{11,12}, with the poly(3,4-ethylenedioxythiophene):poly(styrenesulfonate) (PEDOT:PSS) being the current state-of-art material. On the other hand, the most regularly used electron transport layer (ETL) materials include certain metal fluorides^{13,14}, n-type inorganic (e.g. TiO_x , ZnO)^{15,16} and organic (e.g. bathocuproine)¹⁷ semiconductors. However, there are several drawbacks concerning the current state-of-the-art buffer layers, leading to decreased OPV stability, arising, for example, from the acidic and hygroscopic character of PEDOT:PSS¹⁸ or the sensitiveness of sol-gel prepared TiO_x to moisture, and also the increased manufacturing cost, since some metal oxides and metal fluorides require high vacuum thermal deposition and therefore are incompatible with roll-to-roll (r2r) processes and thus with flexible photovoltaics. In addition, the majority of the aforementioned materials do not allow their work function (WF) tuning,¹⁹ preventing the direct energy match with the numerous active layer donors and acceptors and urging the need for universal, tuned WF buffer layer materials.

Recently, graphene oxide (GO), a graphene sheet functionalized with oxygen groups (e.g. epoxy, hydroxyl, carboxyl), and its derivatives have been investigated as alternatives HTLs and ETLs^{20,21,22,23,24}. The availability of the reactive groups on GO sheets enables its further functionalization with molecules, manipulating in this way its optoelectronic properties^{25,26}. In addition, the solution processable character of GO²⁷ and its derivatives is in accordance with the r2r mass fabrication processes, that are often cited as the advantage of OPVs compared to conventional photovoltaic technologies. More importantly, its tunable WF character makes GO an ideal precursor for creating new materials with WF values perfectly matching the HOMO level of the donor material (a conjugated polymer) and the LUMO level of the acceptor material (usually fullerene derivative). So far, only one study have investigated the photovoltaic performance of devices incorporating simultaneously GO derivatives as HT and ET layers, demonstrating 16% increase in the power conversion efficiency (PCE).²⁸ Nevertheless, the lack of WF tunability of the produced GO derivatives limits its application on only the well-studied poly(3-hexylthiophene-2,5-diyl) (P3HT): [6,6]-phenyl-C61-butyric acid methyl ester ($PC_{61}BM$) based cell, since hole or electron transport is not energetically possible with the current cutting edge active layers, such as poly({4,8-bis[(2-

ethylhexyl)oxy]benzo[1,2-b:4,5-b']dithiophene-2,6-diyl}{3-fluoro-2-[(2-ethylhexyl)carbonyl]thieno[3,4-b]thiophenediyl}} (PTB7): [6,6]-phenyl-C71-butyric acid methyl ester (PC₇₁BM). Therefore low-cost, high-throughput, facile and r2r compatible methods for WF tuning of the GO buffer layers, which will allow their application in high efficient BHJ OPVs are highly desirable.

In this work, a novel, all graphene-based buffer layer OPV device is realized, investigating the effect of the simultaneously utilization of two different solution processable functionalized GOs as cathode and anode buffer layers, on the PCE of the device. The two r2r compatible graphene-based materials, previously prepared by our group, the first one through laser-induced doping of GO with chloride (GO-Cl) leading to a WF increase from 4.9 to 5.16 eV and 5.23 eV and the second one after a simple and fast functionalization of GO with Li alkali metal (GO-Li) leading to a WF decrease from 4.9 to 4.3 eV, exploited unique electron and hole blocking (or transport) properties respectively. The increased WF of GO-Cl and on the other hand the reduced surface potential of GO-Li provide a direct match with the HOMO level of the donor PTB7 and the LUMO level of the acceptor PC₇₁BM respectively, leading to enhanced photovoltaic performance, outperforming by ~19% the reference graphene free device. To our knowledge, the achieved PCE is the highest reported for all graphene based buffer layers OPV devices, opening new paths to develop a new generation of low cost, high efficient, solution processable all-carbon solar cells.

Experimental Section

Preparation of Graphene Oxide (GO):^{29,30} GO was prepared from purified natural graphite powder (Alfa Aesar, ~200 mesh) according to a modified Hummers' method. Specifically, graphite powder (0.5 g) was placed into a cold mixture of concentrated H₂SO₄ (40 mL, 98%) and NaNO₃ (0.375 g) under vigorous stirring for 1 h, in an ice bath. KMnO₄ (3 g) was slowly added into the reaction mixture over 1 h. The mixture was then stirred at room temperature for 4 h. Thereafter, the reaction mixture was allowed to reach room temperature before being heated to 35 °C for 30 min, forming a thick paste. It was then poured into a beaker containing 50 mL of deionized water and further heated to 90 °C for 30 min. 200 mL of distilled water was added, followed by a slow addition of H₂O₂ (3 mL, 30%), turning the color of the solution from dark brown to yellow. The reaction mixture was then allowed to settle down and decanted. The graphite oxide obtained was then purified by repeated high-speed centrifugation (4200 rpm, 3 min) and redispersing in deionized water to neutralize the pH (~10 times needed). Finally, the resulting GO was dried at 60 °C in a vacuum oven for 48 h.

*Preparation of photochlorinated graphene oxide (GO-Cl) films:*²³ The as-spun GO layers on ITO/glass substrates were subjected to irradiation by a KrF excimer laser source emitting 20 ns pulses of 248 nm at 1 Hz repetition rate that was translated onto the film area. For uniform exposure of the whole sample to laser radiation, a top-flat beam profile of 20×10 mm² was obtained using a beam homogenizer. The whole process took place into a vacuum chamber at 50 Torr Cl₂ gas pressure maintained through a precision micro valve system. Different combinations of laser powers (P) and number of pulses (NP) were tested in an effort to optimize the photochemical functionalization processes. In a typical experiment, the sample was irradiated at a constant P with Np=10, 20, 30, 40, 50, 60, 120, 600 and 1200, corresponding to different photochemical reaction times.

*Preparation of graphene oxide functionalized with lithium (GO-Li):*²⁴ The chemical functionalization of GO with lithium was performed using an aqueous solution of the previously prepared GO (1.5 mg mL⁻¹, 40 mL). Li₂CO₃ (200 mg) was then added, and the solution was stirred for 1 h. A polyvinylidene fluoride membrane (0.45 μm) was used to filter and collect the solid, which was then dissolved in water (20 mL). The process of solution and filtration was repeated twice.

*Preparation of the titanium suboxide (TiO_x) solution:*³¹ Titanium(IV) isopropoxide {Ti[OCH(CH₃)₂]₄, 5 mL}, 2-methoxyethanol (CH₃OCH₂CH₂OH, 20 mL), and ethanolamine (H₂NCH₂CH₂OH, 2 mL) were added to a three-neck flask under a nitrogen atmosphere. The solution was then stirred for 1 h at room temperature, followed by heating at 80 °C for 1 h and 120°C for an additional 1 h. The solution was then cooled to room temperature, and 10 mL of methanol was added.

OPV device fabrication: PCDTBT:PC₇₁BM were dissolved in 1,2-dichlorobenzene:chlorobenzene (3:1) (o-DCB:CB) with a 1:4 (4 mg:16 mg) ratio. A PTB7:PC₇₁BM 1:1.5 (10 mg:15 mg) ratio was dissolved in chlorobenzene, followed by the addition of 1,8-diiodooctane (DIO) to give overall DIO amount of 3%. The photovoltaic devices reported were fabricated on 20 mm by 15 mm indium-tin-oxide (ITO) glass substrates with a sheet resistance of ~20 Ω sq⁻¹. The impurities were removed from the ITO glass through a three-step cleaning process (detergent deionized water, acetone, isopropanol). Before the deposition of the hole transport layer (HTL), the substrates were placed inside a ultraviolet ozone cleaner in order to remove the organic contamination and increase the surface hydrophilicity of ITO-coated substrates. The PEDOT:PSS (AI 4083) HTL, purchased from Heraeus, was spin-cast from an aqueous solution on the ITO substrate at 6000 rpm for 60 s and the average thickness of the layer was 30 nm, followed by baking for 15 min at 120 °C inside a nitrogen-filled glove box. All photoactive layers were subsequently deposited by spin-coating the blend solutions at 1000 rpm on top of PEDOT:PSS, GO and GO-Cl

layers. Then the electron extraction layers were coated by spin casting the solutions on top of the active layers. The TiOx interlayer was dissolved in methanol (1:200) and then spin coated to a thickness of approximately 10 nm (6000 rpm, 40 s) in air. GO and GO-Li interlayers were deposited through spin coating at 2000 rpm for 60 s and both controlled to be 2 ± 0.3 nm thick. The devices with PCDTBT:PC₇₁BM blend were then heated at 80 °C for 1 min in air, while the PTB7:PC₇₁ BM-based devices were dried inside a vacuum antichamber with dynamic vacuum for ≈ 15 min. Lastly, 100 nm of Al was deposited, at a standard rate of 1.5 Å/s, through a shadow mask by thermal evaporation on the devices through a shadow mask to define an active area of 4 mm² for each device.

The performances of the devices were measured at room temperature with an Air Mass 1.5 Global (A.M. 1.5 G) solar simulator at an intensity of 100 mWcm⁻². A reference monocrystalline silicon solar cell from Newport was used to calibrate the light intensity. The external quantum efficiency measurements were conducted immediately after device fabrication using an integrated system (Enlitech, Taiwan) and a lock-in amplifier with a current preamplifier under short-circuit conditions. The light spectrum was calibrated using a monocrystalline photodetector of known spectral response. The OPV devices were measured using a Xe lamp passing through a monochromator and an optical chopper at low frequencies (~ 200 Hz) in order to maximize the signal/noise (S/N) ratio. The spot size of the incident monochromatic light was absolute equal with device active area

Results and Discussion

Work function tuning

The as synthesized through the modified Hummers method GO was used as the pristine material to perform the functionalization and the subsequent WF tuning. In particular, the as-spun GO layers on ITO/glass substrates were subjected to irradiation by a KrF excimer laser source emitting 20 ns pulses of 248 nm at 1 Hz repetition rate in the presence of chlorine (Cl₂) precursor gas. To implement and investigate the GO WF tuning, different number of pulses (N_p) was used, increasing from 1 to 65. **Figure 1a** presents the GO WF change with respect to the applied N_p . It is clear that the WF increases as the exposure is more intense, and tends to saturate at 5.23 eV for $N_p=60$, because after this point the level of reduction tends to be very important in the tradeoff between the reduction and doping. In particular, the polar character of C-Cl bonds induced by the formation of surface C^{δ+}-Cl^{δ-} dipoles owing to the different electronegativity between carbon and chloride (2.55 for C

compared to 3.16 for Cl) is responsible for the Fermi level downward shift towards the valence band of GO-Cl, and the subsequent increase in the WF.^{32,33} Thus, this simultaneous chloride doping²⁰ and the partial reduction process³⁴ gives the possibility of wide a WF tuning allowing the use of GO-Cl as a universal HTL in different optoelectronic devices. **Figure 1b** demonstrates such dipoles formation in the C-Cl covalent bonds at the edges and/or Cl-C=O groups located outside the graphene basal plane.³²

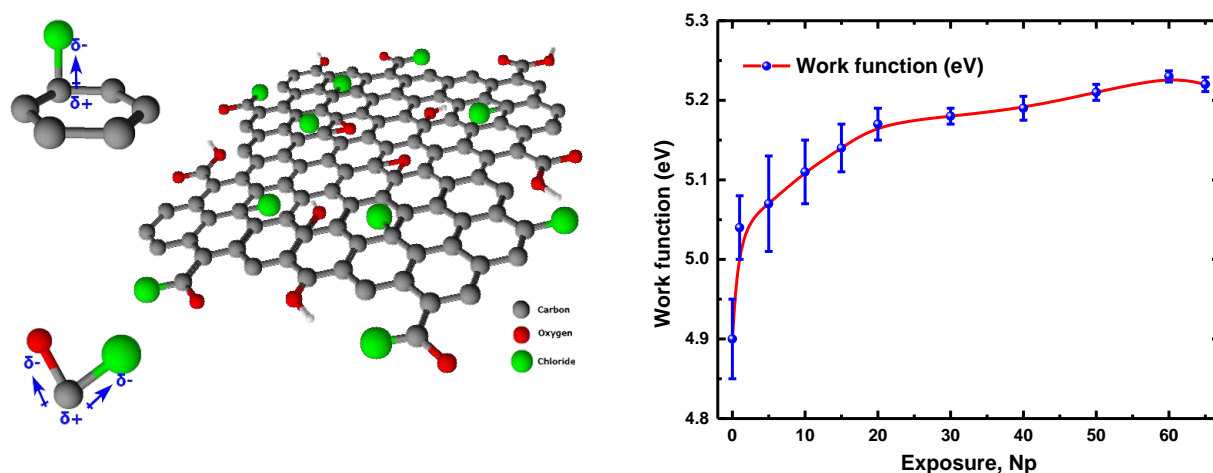


Figure 1. a) Work function tuning of GO-Cl films as a function of the N_p exposure. b) 3D chemical structure of the photochlorinated GO, illustrating the formation of $C^{\delta+}-Cl^{\delta-}$ dipoles.

In contrast to laser induced chloride doping of GO, the replacement of -H in the carboxyl groups of GO with Li atoms can effectively reduce the WF of GO. The GO doping was performed using lithium carbonate (Li_2CO_3) as a precursor. Lithium has low electronegativity value and low WF (2.9 eV). When bonded in GO, Li atoms lose their valence electrons to the GO plane, with the resulted positive Li^+ inducing dipoles.³⁵ The generated charge transfer from the metal to the GO plane lead to an upward shift of the Fermi level toward the vacuum, yielding a difference in the Fermi level between the two materials of 0.68 eV, which is responsible for the WF decrease to $\sim 4.3 \pm 0.1$ eV as depicted in the ultraviolet photoelectron spectra (UPS) (**Figure 2a**) establishing GO-Li as an ideal candidate ETL material for OPVs, since its WF perfect matches the LUMO level of the state of the art electron acceptor materials ($PC_{71}BM$). **Figure 2b** summarizes our findings on GO functionalization to produce GO-based materials with tunable WF (increased or decreased) values with respect to the pristine materials to be used in a variety of optoelectronic applications.

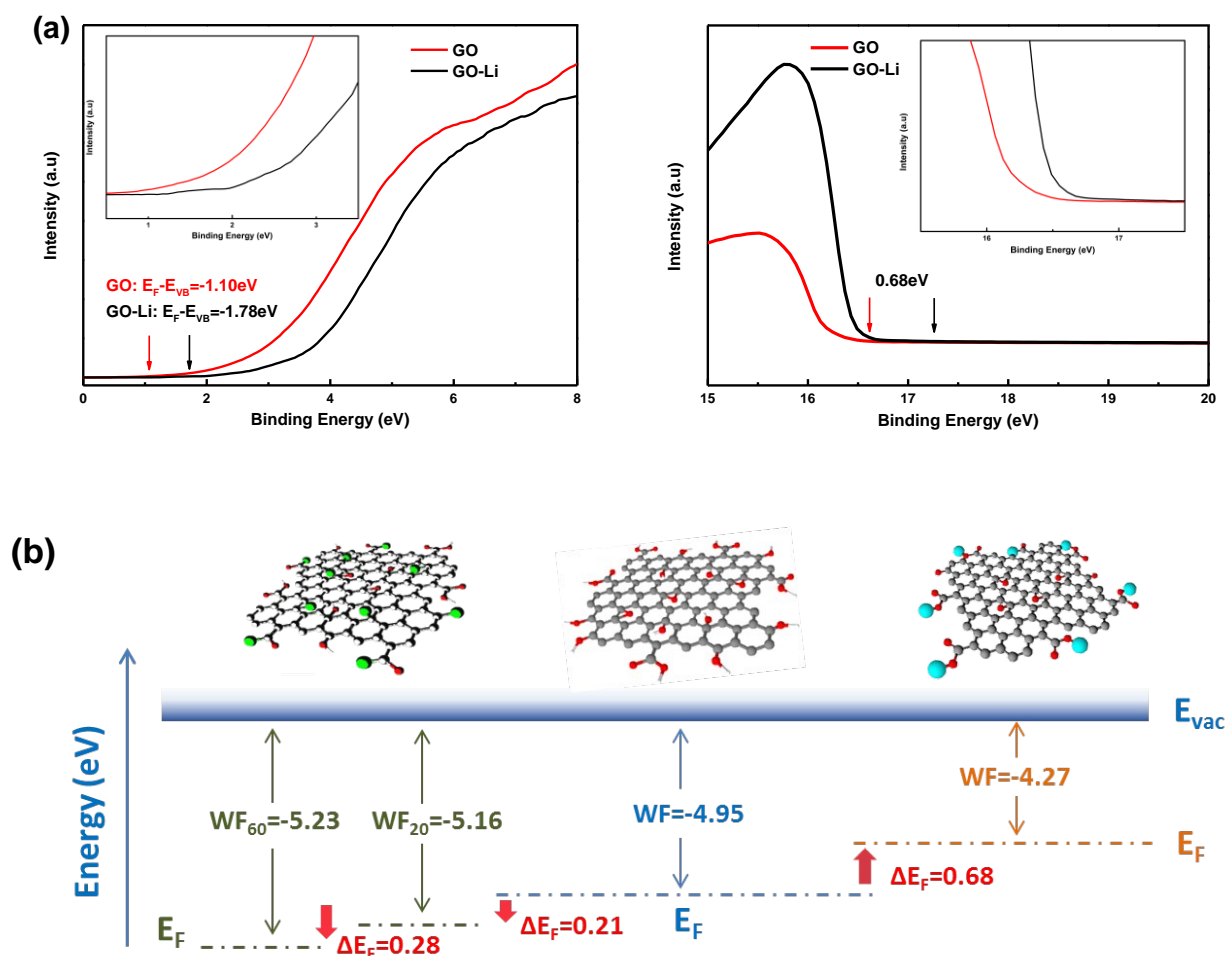


Figure 2. a) UPS valence (right) band region (the inset represents the expanded view of the shallow valence features) and secondary cutoff (left) region for GO and GO-Li (expanded view of the secondary cutoff region features). b) Energy diagram showing the Fermi level of GO (middle) and its shifting after the functionalization with Cl (left) and Li alkali metal (right). In the case of photochlorination different WF values can be achieved by controlling the number of pulses (in this case $N_p=20$ or 60).

Photovoltaic performance

To assess the viability of the proposed GO WF tuning methods in optoelectronic applications, different structures of PCDTBT:PC₇₁BM and PTB7:PC₇₁BM-based OPV devices were fabricated. More particular, the effects by the incorporation of GO-Cl (with different WF values) as HTL and the GO-Li as ETL on device performance were investigated and compared with the state of the art buffer layer materials (PEDOT:PSS and TiO_x as HTL and ETL respectively). The device structure and the energy level diagrams of the different materials used in this study are shown in **Figure 3**.

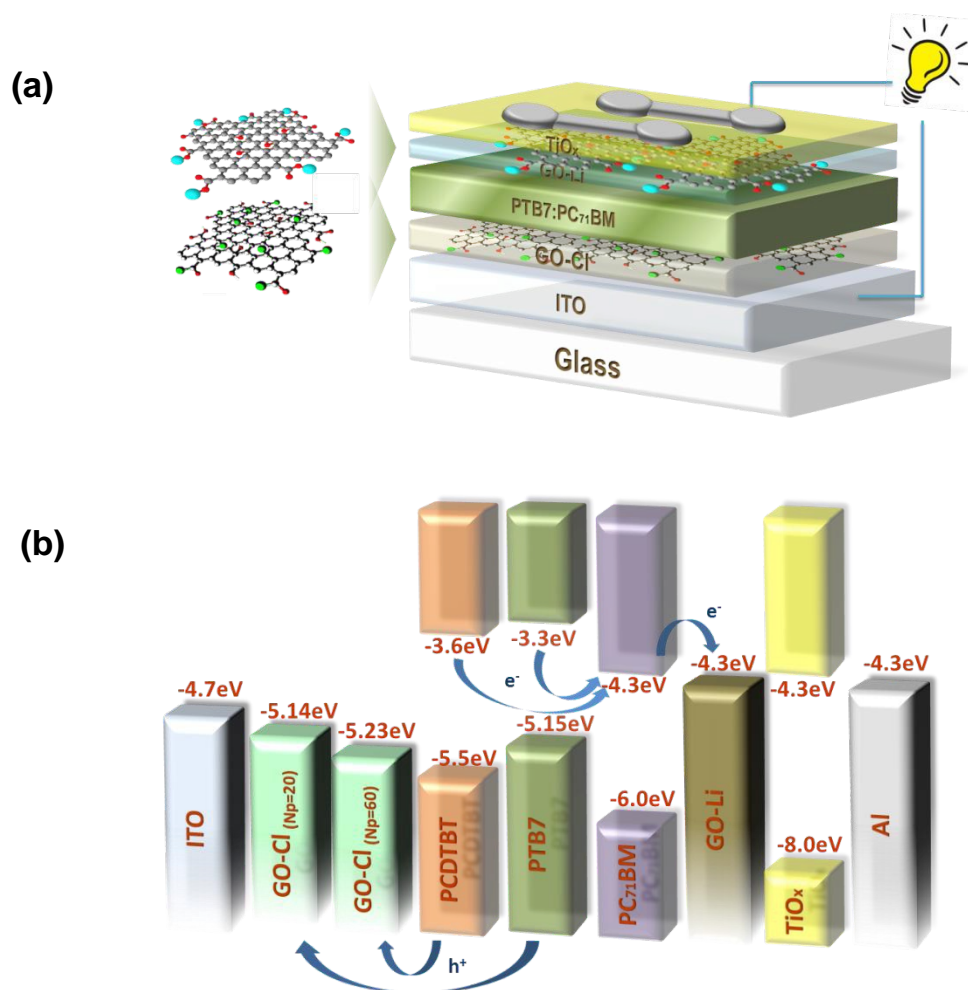


Figure 3. a) Schematic illustration of the BHJ OPV device with GO-Cl as the HTL and GO-Li/TiO_x as the ETL. b) Energy level diagram depicting the relevant energy levels under flat conditions of all materials used in OPV cells studied and not the actual interfaces.

The averaged photovoltaic characteristics obtained from 10 identical devices, consisting of 6 cells each (60 current density-voltage (J-V) curves in total) are summarized in **Table 1**, indicate that the incorporation of GO-Cl as HTL and GO-Li as ETL significantly increases the device efficiency by ~12% and ~8% compared to the reference device (PEDOT:PSS as HTL and TiO_x as ETL). As depicted in **Figure 3b**, the proposed laser induced technique for WF tuning, allowed to produce universal graphene-based HT material with desirable electronic properties. In particular, OPV devices with two different polymer donors a) PCDTBT with HOMO of 5.5 eV and b) PTB7 with HOMO of 5.15 eV were fabricated to clarify the effect of the use of GO-Cl with different WF values on photovoltaic performance. **Figure 4a** demonstrates the typical illuminated (100 mW cm⁻²) J-V curves of the PCDTBT:PC₇₁BM OPV devices incorporating PEDOT:PSS, GO and GO-Cl with different WF as HTLs. A significant enhancement in the photovoltaic performance upon the increase of GO-Cl WF values can be observed, leading to a PCE of

6.56% for GO-Cl (5.23 eV) compared to the references devices with PEDOT:PSS (5.49%) and GO (5.59%) HTLs, which can be attributed to the improved hole transport as verified by the hole mobility measurements.²⁰ The universal applicability of the proposed method is demonstrated by the fact that the less laser exposed GO-Cl sample exhibiting WF of 5.16 eV ($N_p = 20$) was used as HTL in PTB7:PC₇₁BM devices achieving a record PCE of 8.28 % for graphene-based HTL devices (**Figure 4b**). This difference in optimum WF value for GO-Cl applied in the two different photoactive blends can be explained by the induced offset between the two donors HOMO level and the WF of the GO-Cl. In particular, for PTB7-based devices using 20 pulses for GO chlorination induces a ~ 0.01 eV energy barrier between the HOMO of the PTB7 and the WF of GO-Cl, while in the PCDTBT case, the corresponding minimum energy barrier is 0.27 eV (**Figure 4c**). Therefore, it can be concluded that the ability to fine tune the GO-Cl WF with respect to the polymer-donor energy levels offers a facile route to boost the OPV PCEs.

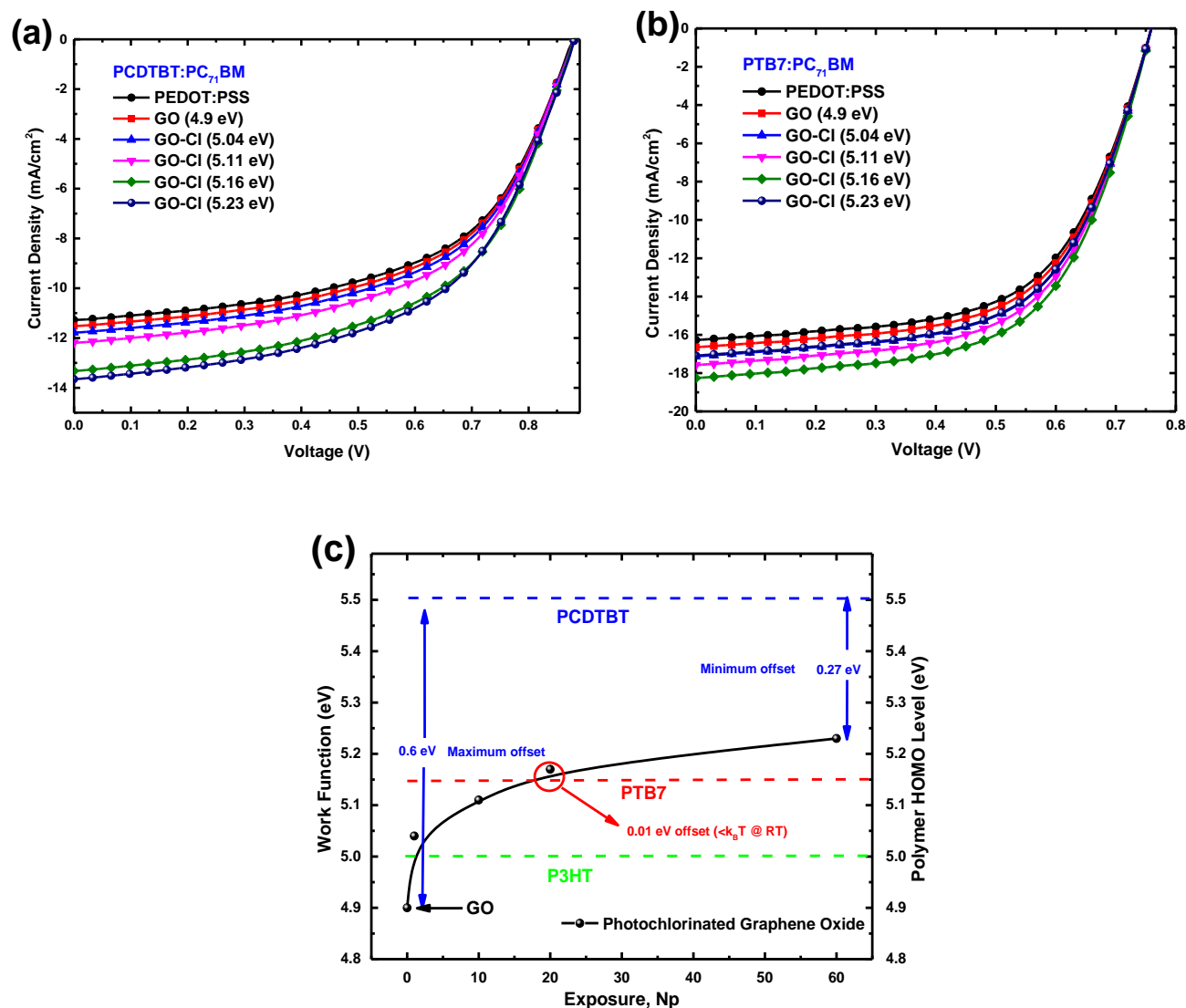


Figure 4. J-V characteristics of a) PCDTBT:PC₇₁BM and b) PTB7:PC₇₁BM-based photovoltaic devices incorporating different HTLs, but the same TiO_x ETL. c) Graph demonstrating the WF tuning of GO-Cl films as a function of the Np exposure and the relevant energy offset between the photochlorination treated films and the polymer donor HOMO level.

Figure 5 shows the illuminated J-V curves of the PCDTBT:PC₇₁BM and PTB7:PC₇₁BM-based OPV devices with TiO_x and GO-Li/TiO_x as ETLs. The reference PCDTBT:PC₇₁BM-based device incorporating TiO_x ETL yielded a PCE of 5.53%, with a short circuit current density (J_{sc}) of 11.28 mA cm⁻², an open circuit voltage (V_{oc}) of 882 mV, and a fill factor (FF) of 55.6%, compared to the GO-Li/TiO_x bilayer ETL based device that yielded a significantly enhanced PCE of 6.25%, with J_{sc} of 12.51 mA cm⁻², V_{oc} of 884 mV, and FF 56.5%. In addition, PCDTBT-based devices were prepared by replacing the GO-Li interfacial layer with GO to better clarify the effect of WF tuning in device efficiency. In this case, a significant decrease of the J_{sc} by ~15% and of the FF by ~9% was observed, which can be attributed to the energy offset of 0.6 eV between the LUMO level of the acceptor material (4.3 ± 0.1 eV) and the GO WF (4.95 ± 0.1 eV). For ideal electron transport, the LUMO level of the acceptor material should be absolute equal to the WF of the ETL. Therefore, as the GO-Li WF perfectly matches the LUMO of PC₇₁BM and TiO_x ETL, the electrons transport to the cathode is conducted without energy barrier. The J_{sc} enhancement can be attributed to the improved electron transportation due to the 2D nature of the GO-Li interfacial ETL. Atomic force microscopy measurements have also verified that GO-Li has a planarizing role,²⁴ creating a perfect interface between the TiO_x ETL and the cathode, leading to an improved Ohmic contact and therefore minimizing the contact resistance at the interface.²⁴ In this context OPV devices were fabricated using PTB7 as polymer donor. After the introduction of GO-Li between the active layer and the TiO_x the device PCE was increased from 7.4% to 7.98%, mainly due to a significant increase in the J_{sc} which is maybe caused by the improve electron extraction as in the case of PCDTBT based devices.²⁴

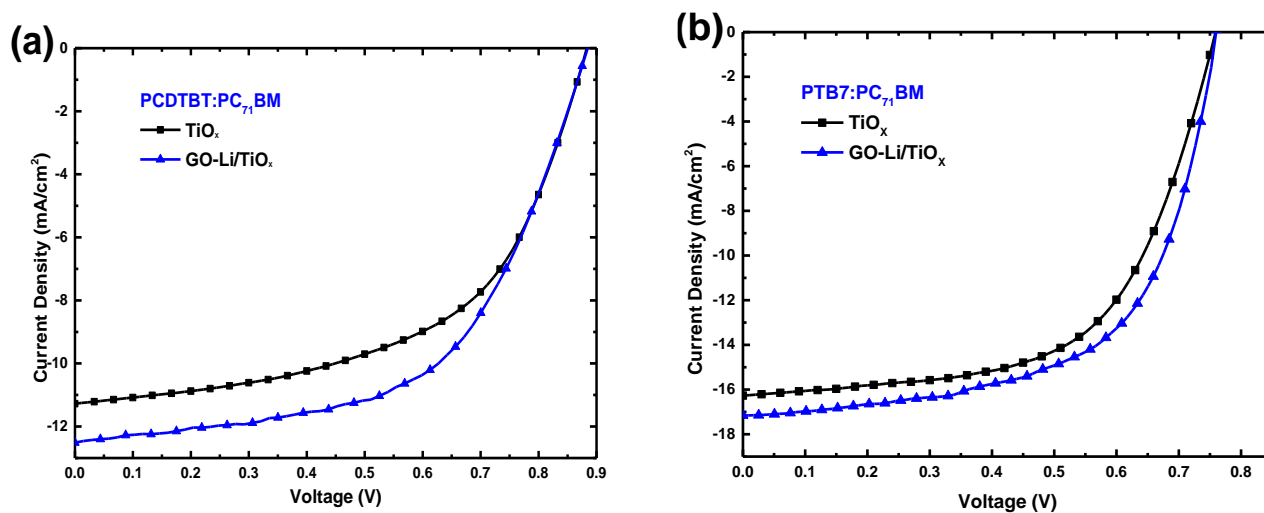


Figure 5. J-V characteristics of a) PCDTBT:PC₇₁BM and b) PTB7:PC₇₁BM-based photovoltaic devices incorporating different ETLs, but the same PEDOT:PSS HTL.

To further support the excellent hole and electron extraction capabilities of GO-Cl and GO-Li respectively, OPV devices incorporating graphene-based materials as both HT and ET layers were fabricated. For this purpose, both the performance of the reference device with the configuration of glass/ITO/PEDOT:PSS/PCDTBT:PC₇₁BM or PTB7:PC₇₁BM/TiO_x/Al and the one structured as glass/ITO/GO-Cl/PCDTBT:PC₇₁BM or PTB7:PC₇₁BM/GO-Li/TiO_x/Al were investigated. **Figure 6** depicts the J-V curves for the tested devices. Clearly, in both BHJ active layer there is a significant J_{SC} improvement (28% for PCDTBT and 18% for PTB7-based devices) upon the addition of graphene-based interlayers. On the one hand, this is because of the WF match between GO-Li and the LUMO level of PC₇₁BM, with the GO-Li modified electrode forming an Ohmic contact with the PCDTBT:PC₇₁BM and PTB7:PC₇₁BM active layer for improved electron extraction. On the other hand, the WF tuning of GO-Cl produces HTL materials that match the HOMO level of PCDTBT and PTB7 ensuring an Ohmic contact at the interface for efficient hole extraction. On the other hand, the alignment of the GO HTL WF to the polymer HOMO, through photochlorination, does not result to a change in the V_{oc}. The maximum V_{oc} of bulk heterojunction OPV devices typically results from the polymer donor and fullerene acceptor interface gap, that is the energy difference between the HOMO of the polymer and the LUMO of the fullerene.^{36,37} In this way, charge transfer leads the WFs of the ETL and the HTL to be pinned to the LUMO of the fullerene and the HOMO of the polymer respectively.³⁸ Therefore, the V_{oc} is unaffected, since regarding the WF of the GO-Cl HTL employed, a Fermi level pinning of the HTL WF to the HOMO of the polymer donor takes place, in full agreement with previous works.^{39,40} On top of that the actual interface between the HTL and the active layer does not change upon the WF tuning process, since the photochlorination takes place on the spin-coated GO films and does not cause any morphological changes. As a result, both graphene-based buffer layers OPV devices significantly outperformed the reference ones, leading to a PCE improvement of 30% for PCDTBT and 19% for PTB7-based devices and to a record PCE of 9.14% for graphene-based buffer layer devices.

The dark J-V curves (**Figure S1**) also show excellent diode characteristics with very low leakage current and high rectification ratio for the combination of both HT and ET graphene based devices (forward to reverse factor higher than 10³) exhibiting that the injected current density in the dark (0.5–1.0 V) is higher than that of the reference device. This is in full agreement with the assumed reduced injection barrier. In order to get an insight for the responsible mechanism of the enhanced device performance, the incident photon-to-electron conversion efficiency (IPCE) curves (**Figure 6c**) of the devices with different buffer layer combinations was measured and compared with the pristine one. The pristine device exhibits a maximum IPCE of ~69%, while the GO-Cl / GO-Li based devices exhibit an enhanced maximum of ~86% using PTB7 as donor

material. This significant and broad enhancement is in agreement with increased J_{sc} observed in the J-V measurements. It should also be noted that, the J_{sc} calculated by integrating the IPCE spectrum with the AM 1.5G spectrum, for the pristine and the GO-Cl / GO-Li based PTB7-PC₇₁BM devices are 15.75 and 18.51 mA cm⁻² respectively. The actual J_{sc} measured from J-V curves were 4% larger than the IPCE calculated values, indicating good accuracy of the OPV measurement. It should be noted that the J-V curves were firstly recorded inside the glove box in encapsulated OPV devices, and moved outside the glove box for the IPCE measurements.

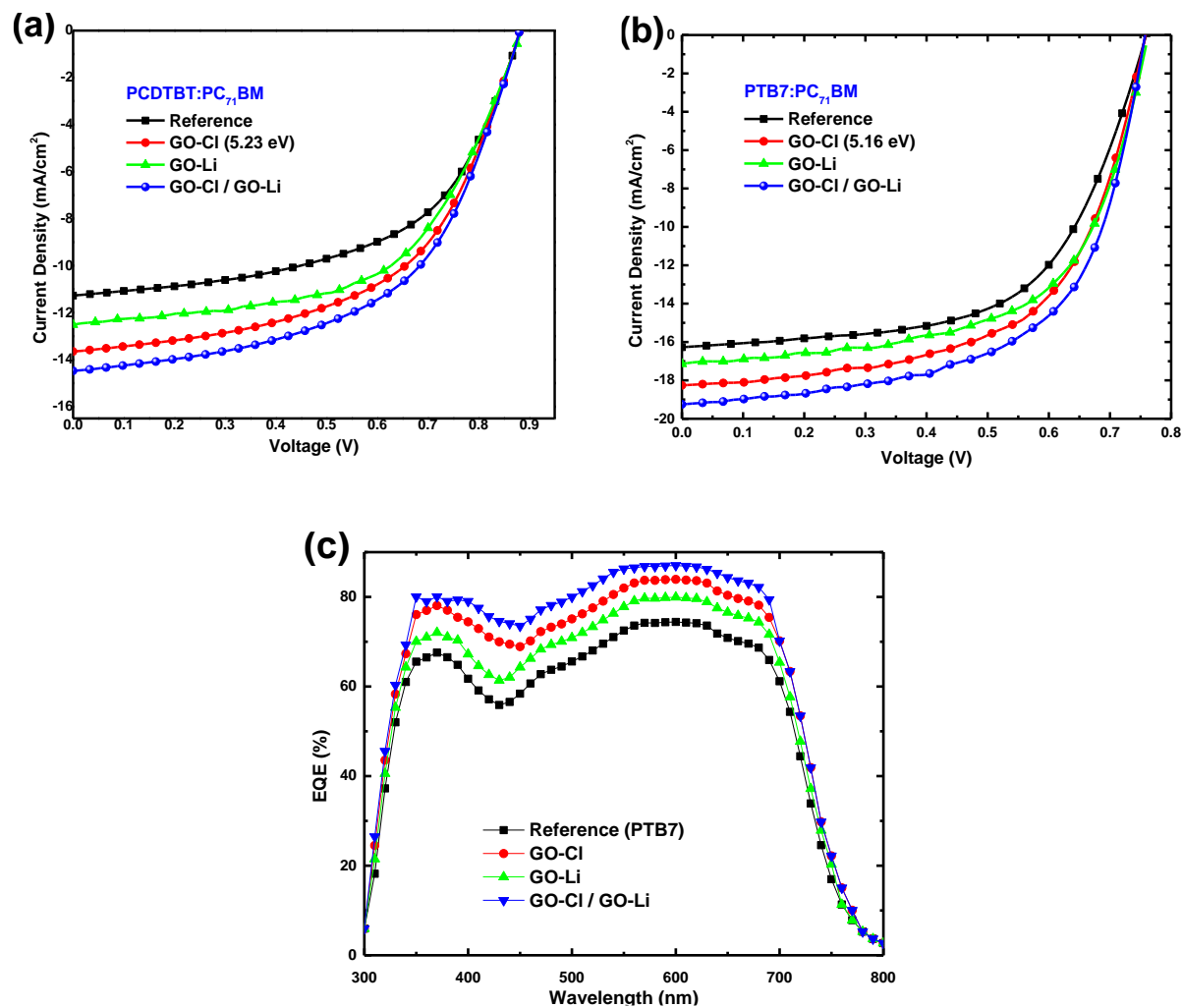


Figure 6. J-V characteristics of a) PCDTBT:PC₇₁BM, b) PTB7:PC₇₁BM-based photovoltaic devices and c) IPCE spectra for the devices using different combinations of hole and electron transport layers of PTB7 based OPV devices.

Table 1. Summary of the averaged photovoltaic parameters of the fabricated OPVs. Devices with two different polymer donors a) PCDTBT with HOMO of 5.5 eV and b) PTB7 with HOMO of 5.15 eV were fabricated. PEDOT:PSS, GO and GO-Cl with different WF values were used and compared with respect to their HTL performance in PCDTBT:PC₇₁BM and PTB7:PC₇₁BM-based photovoltaic devices incorporating the same TiO_x ETL. In addition, TiO_x, GO/TiO_x and GO-Li/TiO_x were used and

compared with respect to their ETL performance in PCDTBT:PC₇₁BM and PTB7:PC₇₁BM-based photovoltaic devices incorporating the same PEDOT:PSS HTL. Finally, combo OPV devices incorporating GO-Cl and GO-Li/TiO_x as HT and ET layers respectively were fabricated and compared with the reference device incorporating PEDOT:PSS and TiO_x as buffer layers.

HTL	J _{sc} (mA cm ⁻²)	V _{oc} (V)	FF (%)	PCE (%)
PCDTBT:PC ₇₁ BM				
PEDOT:PSS	11.28±0.12	0.880±0.02	55.6±0.3	5.51 (5.61)
GO	11.52±0.15	0.880±0.02	55.1±0.4	5.59 (5.71)
GO-Cl (5.04 eV)	11.78±0.14	0.880±0.02	55.1±0.3	5.71 (5.82)
GO-Cl (5.11 eV)	12.19±0.17	0.880±0.02	55.2±0.5	5.92 (6.07)
GO-Cl (5.16 eV)	13.32±0.15	0.880±0.02	55.1±0.5	6.46 (6.61)
GO-Cl (5.23 eV)	13.65±0.19	0.880±0.02	55.3±0.4	6.57 (6.79)
PTB7:PC ₇₁ BM				
PEDOT:PSS	16.27 ±0.23	0.760±0.03	59.8±0.6	7.40 (7.60)
GO	16.65±0.21	0.760±0.03	59.7±0.5	7.56 (7.74)
GO-Cl (5.04 eV)	17.13±0.18	0.760±0.02	59.6±0.5	7.78 (7.93)
GO-Cl (5.11 eV)	17.58±0.25	0.760±0.03	59.6±0.6	7.97 (8.19)
GO-Cl (5.16 eV)	18.30±0.27	0.760±0.02	59.9±0.8	8.28 (8.52)
GO-Cl (5.23 eV)	17.09±0.19	0.760±0.03	59.5±0.05	7.73 (7.91)
ETL	J _{sc} (mA cm ⁻²)	V _{oc} (V)	FF (%)	PCE (%)
PCDTBT:PC ₇₁ BM				
TiO _x	11.28±0.12	0.882±0.02	55.6±0.3	5.53 (5.61)
GO/TiO _x	10.73±0.19	0.883±0.05	51.6±0.3	4.89 (5.03)
GO-Li/TiO _x	12.51±0.35	0.884±0.05	56.5±0.5	6.25 (6.57)
PTB7:PC ₇₁ BM				
TiO _x	16.27±0.23	0.760±0.03	59.8±0.6	7.39 (7.60)
GO/TiO _x	15.32±0.31	0.757±0.02	54.8±0.8	6.35 (6.60)
GO-Li/TiO _x	17.16±0.25	0.759±0.02	61.2±0.5	7.98 (8.17)
Combo	J _{sc} (mA cm ⁻²)	V _{oc} (V)	FF (%)	PCE (%)
PCDTBT:PC ₇₁ BM				
PEDOT:PSS & TiO _x	11.28±0.12	0.878±0.02	55.6±0.3	5.51 (5.61)
GO-Cl & GO-Li/TiO _x	14.48±0.13	0.880±0.01	56.3±0.5	7.17 (7.31)
PTB7:PC ₇₁ BM				
PEDOT:PSS & TiO _x	16.27±0.23	0.760±0.03	59.8±0.6	7.39 (7.60)
GO-Cl & GO-Li/TiO _x	19.28±0.31	0.760±0.02	60.5±0.7	8.83 (9.14)

*Average photovoltaic characteristics and standard deviations for the different structured OPV devices. The numbers in parentheses represent the values obtained for the champion OPV cells. To account for experimental errors, the reported averages and deviations for each ETL are taken for 10 identical devices, consisting of six cells each.

The increased value of J_{sc} was also investigated through electron and hole mobility measurements (**Figure S2**). For that purpose electron- and hole-only devices were fabricated with the following structure: ITO/HTL/Active layer/ETL/Au for the hole-only and ITO/Al/HTL/Active layer/ETL/Al for the electron only device respectively. The values calculated were improved for both electron and hole mobilities. Calculations were based on Mott–Gurney equation:

$$J_{SCLC} = \frac{9}{8} \epsilon_r \epsilon_0 \mu \frac{(V - V_{bi})^2}{d^3}$$

in which ϵ_r is the relative dielectric constant, ϵ_0 is the permittivity of free-space, μ is the charge carrier mobility, V is the applied voltage, V_{bi} is the built-in potential and d is the thickness of the active layer. The mobility values for the reference OPV device were $\mu_e = 7.86 \times 10^{-5} \text{ cm}^2 \text{ V}^{-1} \text{ s}^{-1}$ for the electron and $\mu_h = 1.30 \times 10^{-4} \text{ cm}^2 \text{ V}^{-1} \text{ s}^{-1}$ for the hole mobility while for the GO-Cl / GO-Li based cells the values were $\mu_e = 1.59 \times 10^{-4} \text{ cm}^2 \text{ V}^{-1} \text{ s}^{-1}$ for the electron and $\mu_h = 1.91 \times 10^{-4} \text{ cm}^2 \text{ V}^{-1} \text{ s}^{-1}$ for the hole mobility, respectively. The mobilities were not only increased, especially the electron mobility, but also balanced which is a very important factor in order to prevent charge accumulation in the device. Before further analyzing our results we should first shed light in the functional mechanism taking place. Because holes are collected at the front electrode in the conventional device structure, and taking into account that the most of the excitons are created near by the front contact the holes mobilities should have slightly lower value compared to the electron mobility. Thus, this is the reason that PTB7 based OPV devices ($\mu_h > \mu_e$) have lower PCE values in the conventional structure compared to the inverted one and in our case this is maybe the reason for the lower PCE enhancement of PTB7 compared to PCDTBT ($\mu_h > \mu_e$). In this context, this is a crucial improvement because electron transport is considered as a factor that limits the photocurrent generation in the conventional PTB7 based devices, since the electron mobility is much lower than the hole mobility. Both electron and hole mobility increases should be attributed on the one hand to GO–Li planaring role²⁴ and perfect energy levels matching and on the other hand to perfect WF tuning of GO after the photochlorination process. As a result, when we combined GO-Cl HTL and GO-Li interfacial layer the μ_h/μ_e ratio was significantly reduced, from 1.65 to 1.20 as it is observed in **Table 2**. We can thus assume, that if we use the inverted structure with the proposed graphene based buffer layers the improvement in the PCE could be much higher than in the conventional structure used here.

Table 2. Electron and hole mobilities of the reference and the device with graphene based buffer layers

HTL / ETL	μ_h (cm ² V ⁻¹ s ⁻¹)	μ_e (cm ² V ⁻¹ s ⁻¹)	Ratio (μ_h / μ_e)
PTB7:PC ₇₁ BM			
PEDOT:PSS / TiO _x	1.30 × 10 ⁻⁴	7.86 × 10 ⁻⁴	1.65
GO-Cl / GO-Li	1.91 × 10 ⁻⁴	1.59 × 10 ⁻⁴	1.20

In order to examine and confirm our findings (increased J_{sc} and balanced mobilities) we studied the charge recombination kinetics at short circuit for the reference and for the devices with graphene based buffer layers. The J_{sc} can be correlated to illumination intensity (I_{light}) by,

$$J_{sc} = \alpha I_{light}^n \quad (n \leq 1)$$

At short circuit, the bimolecular recombination should be minimum ($n < 1$) for maximum carrier sweep out. Any deviation from a < 1 implies bimolecular recombination⁴¹. **Figure S3** shows J_{sc} vs. I fitted using the power law described above. The fitting of the data yield $a=0.870$ for reference device, which can be attributed to bimolecular recombination. After the introduction of GO-Cl and GO-Li, a is 0.968, which imply that bimolecular recombination is significantly reduced. To gain further insight into the origin of the enhanced J_{sc} in the device, one-dimensional transfer matrix formalism based on optical modeling calculations assuming monochromatic light propagating normal to the device layers was conducted.⁴² **Figure 7** presents the simulated optical electric field distribution, $|E^2|$, as a function of wavelength in the reference OPV device and using different combinations of buffer layer as reported previously. The optical constants of the PCDTBT:PC₇₁BM layer were obtained from previous reports.⁴³ As shown in **Figure 7**, the optical electric field amplitude is significantly enhanced for the device with the GO-Li interfacial layer and GO-Cl as HTL, compared with that of the reference device with only the TiO_x as ETL and with PEDOT:PSS as HTL. The highest optical electric field amplitudes are 0.745 and 0.619 for the dual graphene based buffer device and reference, respectively. This electric field enhancement is directly attributed to the better refractive index (n) matching in the sandwich devices using graphene based buffer layer compared to the reference sandwich. In particular, for the reference device PEDOT:PSS n value is ~ 1.5 , PTB7:PC₇₁BM is ~ 1.9 and TiO_x ~ 2.5 and for the graphene based buffer layer device GO-Cl n value is ~ 1.9 , PTB7:PC₇₁BM is ~ 1.9 GO-Li is ~ 2 and TiO_x is ~ 2.5 . In this way, an important part of the incident electric field is reflected at the interface between PEDOT:PSS and active layer while in the case of GO-Cl due to the perfect n matching the interface parasitic reflection is minimum. Also, GO-Li n matches with the n of active layer and TiO_x

acting as a bridge gradually allowing the electric field to pass through the device and thus increasing its intensity.⁴⁴ We can conclude that the addition of the graphene based buffer layers increases the electric field amplitude in the photoactive layer, and therefore, more photocurrent is generated in the devices. This effect acts in synergy with the observed balanced charge mobilities. Therefore, the enhancement in PCE upon the addition of a GO-Li interfacial layer and GO-CI HTL can be attributed to the observed reduced recombination at the interfaces, balanced charge mobilities, and enhanced electric field in the device.

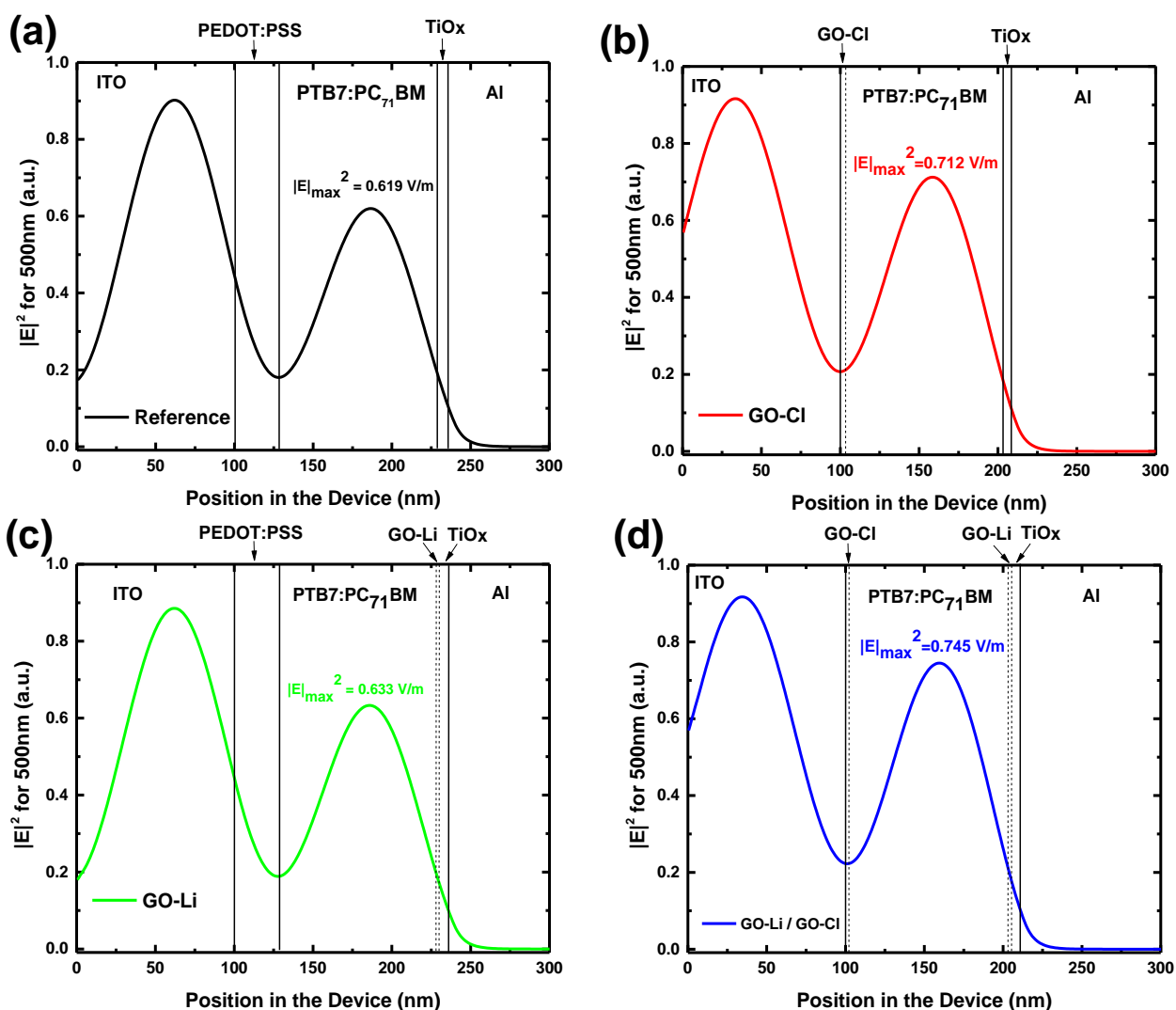


Figure 7. Calculated distribution of the normalized modulus squared of the optical electric field $|E|^2$ inside an OPV device: a) ITO (100 nm)/PEDOT:PSS (35 nm)/PTB7:PC₇₁BM (100 nm)/TiOx (10 nm)/Al (100 nm), b) ITO (100 nm)/GO-CI (2 nm)/PTB7:PC₇₁BM (100 nm)/TiOx (10 nm)/Al (100 nm), c) ITO (100 nm)/PEDOT:PSS (35 nm)/PTB7:PC₇₁BM (100 nm)/GO-Li(2 nm)/TiOx (10 nm)/Al (100 nm) and d) ITO (100 nm)/GO-CI (2 nm)/PTB7:PC₇₁BM (100 nm)/GO-Li(2 nm)/TiOx (10 nm)/Al (100 nm) for a wavelength of 500 nm.

It is important to note that the significant transparencies difference ($\sim 12\%$, Figure S4) between the PEDOT:PSS and graphene-based HTLs increases the exciton generation (G) in the active layer, which is clearly indicated by the improvement of the maximum $|E|^2$ (Figure 7a,b). By increasing the HTL transparency, the incident light reaching the active layer also increases, leading to improved G. Considering that $|E|^2$ is proportional to G^{45} , graphene-based HTL devices would exhibit much higher IPCE values, as verified in IPCE measurements presented in Figure 6c. In summary, the increased HTL transparency acts in synergy with the better refractive index matching between the graphene-based HTL and ETLs and the PTB7:PC₇₁BM active layer, leading to the $\sim 20\%$ improvement in $|E|^2$. Taking also into account that graphene-based buffer layers improves the charge carrier mobilities of the OPV device, it is expected that the respective charge collection would be much higher than the PEDOT:PSS HTL and the neat TiO_x ETL based devices. The above support the improved IPCE values for the graphene-based devices.

To further verify the EQE enhancement mechanisms, the internal quantum efficiency (IQE) spectra were calculated using the optical model as follows. Firstly, the absorption spectrum, extracted from the reflection spectrum (R) by $1-R$, assuming that Al back contact is a perfect mirror of the devices with different materials used as buffer layers, was derived from the optical modeling, taking into account that the absorption is mainly from the active layer. The IQE of the devices was deduced from EQE (Figure 6c) and reflected absorption (Figure S5a) respectively⁴⁶. It can be observed that the combo device IQE (Figure S5b) is enhanced compared to the reference device due to a) the balanced charge carrier mobilities (Table 2), b) the reduced bimolecular recombination (Figure S3) when GO-Cl and GO-Li were used as HT and ET layers and c) the improved n matching of the two graphene-based buffer layers with the photoactive blend. It is worth to note that in the regions in which the PTB7:PC71BM absorption coefficient is maximum, the IQE presents a significant improvement reaching a maximum of $\sim 97\%$, further supporting the fact that the WF matching of the buffer layers with the donor and acceptor energy levels, contribute to highly efficient charge carriers collection per incident absorbed photon. Moreover, the calculated IQE peak is less than the 100% theoretical maximum, ensuring that the calculations were accurate. Moreover, the calculated IQE peak is less than the 100% theoretical maximum, ensuring that the calculations were accurate.

Conclusion

In summary, this work demonstrates how the WF tuning of the buffer layers can affect the performance of OPV devices. Two facile, fast, non-destructive and r2r compatible methods are briefly presented, which allowed the WF fine tuning of

graphene-based derivatives to develop universal buffer layers that directly match the energy levels of the polymer donor and electron acceptor in the state-of-the-art OPVs. OPVs with a GO-Cl as HTL exhibited a PCE of 8.28%, much higher than those of reference devices with GO (7.56%) or PEDOT:PSS (7.40%), while the incorporation of GO-Li as ET interlayer between the active layer and the TiO_x optical spacer led to a PCE of 7.98% which was significantly increased compared to the reference one (7.40%). The excellent hole and electron extraction capabilities of GO-Cl and GO-Li were combined to an all graphene-based buffer layer OPV device which exhibited a PCE of 9.14% (8.83% average), significantly outperforming the reference one by ~19%. The described methods can contribute to novel interface engineering approaches, creating graphene- and other 2D materials-based derivatives as excellent potential candidates for a wide range of new applications with tunable optoelectrical properties, including flexible electronic OPVs, perovskite solar cells, organic light emitting diodes, and photosensors, as well as traditional electronic devices.

Acknowledgements

The research leading to these results has received funding from the European Union Seventh Framework Programme under Grant Agreement No. 604391 Graphene Flagship.

References

- ¹ B. C. Thompson, J. M. J. Frechet, *Angew. Chem., Int. Ed.*, 2007, **47**, 58
- ² B. Azzopardi, C. J. M. Emmott, A. Urbina, F. C. Krebs, J. Mutale, J. Nelson, *Energy Environ. Sci.*, 2011, **4**, 3741
- ³ G. Li, R. Zhu, Y. Yang, *Nat. Photonics*, 2012, **6**, 153
- ⁴ J. Adams, G. D. Spyropoulos, M. Salvador, N. Li, S. Strohm, L. Lucera, S. Langner, F. Machui, H. Zhang, T. Ameri, M. M. Voigt, F. C. Krebs, C. J. Brabec, *Energy Environ. Sci.*, 2015, **8**, 169
- ⁵ J. B. You, L. T. Dou, K. Yoshimura, T. Kato, K. Ohya, T. Moriarty, K. Emery, C. C. Chen, J. Gao, G. Li, Y. Yang, *Nat. Commun.*, 2013, **4**, 1446
- ⁶ R. Steim, F. R. Kogler, C. J. Brabec, *J. Mater. Chem.*, 2010, **20**, 2499
- ⁷ H. Ma, H. L. Yip., F. Huang, A. K. Y. Jen, *Adv. Funct. Mater.*, 2010, **20**, 1371
- ⁸ C.-Z. Li, C.-Y. Chang, Y. Zang, H.-X. Ju, C.-C. Chueh, P.-W. Liang, N. Cho, D. S. Ginger and A. K. Y. Jen, *Adv. Mater.*, 2014, **26**, 6262
- ⁹ V. Shrotriya, G. Li, Y. Yao, C. Chu, Y. Yang, *Appl. Phys. Lett.*, 2006, **88**, 073508
- ¹⁰ M. D. Irwin, D. B. Buchholz, A. W. Hains, R. P. H. Chang, T. J. Marks, *Proc. Natl. Acad. Sci. U.S.A.*, 2008, **105**, 2783

- ¹¹ H. Yan, P. Lee, N. R. Armstrong, A. Graham, G. A. Evmenenko, P. Dutta, T. J. Marks, *J. Am. Chem. Soc.*, 2005, **127**, 3172
- ¹² A. W. Hains, T. J. Marks, *Appl. Phys. Lett.*, 2008, **92**, 023504
- ¹³ X. Jiang, H. Xu, L. Yang, M. Shi, M. Wang, H. Chen, *Sol. Energy Mater. Sol. Cells*, 2009, **93**, 650
- ¹⁴ C. J. Brabec, S. E. Shaheen, C. Winder, N. S. Sariciftci, *Appl. Phys. Lett.*, 2002, **80**, 1288
- ¹⁵ J. Y. Kim, S. H. Kim, H. H. Lee, K. Lee, W. Ma, X. Gong, A. J. Heeger, *Adv. Mater.*, 2006, **18**, 572
- ¹⁶ H. L. Yip, S. K. Hau, N. S. Baek, H. Ma, A. K.Y. Jen, *Adv. Mater.*, 2008, **20**, 2376
- ¹⁷ T.Y. Chu, J. Lu, S. Beaupre, Y. Zhang, J.R. Pouliot, S. Wakim, J. Zhou, M. Leclerc, Z. Li, J. Ding, Y. Tao, *J. Am. Chem. Soc.*, 2011, **133**, 4250
- ¹⁸ M. Jorgensen, K. Norrman, F. C. Krebs, *Sol. Energy Mater. Sol. Cells*, 2008, **92**, 686
- ¹⁹ L. Lu, T. Xu, I. H. Jung, L. Yu, *J. Phys. Chem. C*, 2014, **118**, 22834-22839
- ²⁰ S.-S. Li, K.-H. Tu, C.-C. Lin, C.-W. Chen, M. Chhowalla, *ACS Nano*, 2010, **4**, 3169-3174
- ²¹ J. Liu, Y. Xue, L. Dai, *J. Phys. Chem. Lett.*, 2012, **3**, 1928-1933
- ²² J.-S. Yeo, J.-M. Yun, Y.-S. Jung, D.-Y. Kim, Y.-J. Noh, S.-S. Kim, S.-I. Na, *J. Mater. Chem. A*, 2014, **2**, 292-298
- ²³ E. Stratakis, K. Savva, D. Konios, C. Petridis, E. Kymakis, *Nanoscale*, 2014, **6**, 6925-6931
- ²⁴ G. Kakavelakis, D. Konios, E. Stratakis, E. Kymakis, *Chem. Mater.*, 2014, **26**, 5988-5993
- ²⁵ T.-Y. Chu, S.-W. Tsang, J. Zhou, P. G. Verly, J. Lu, S. Beaupré, M. Leclerc, Y. Tao, *Sol. Energy Mater. Sol. Cells*, 2012, **96**, 155
- ²⁶ C. A. Amb, S. Chen, K. R. Graham, J. Subbiah, C. E. Small, F. So, J. R. Reynolds, *J. Am. Chem. Soc.* 2011, **133**, 10062
- ²⁷ D. Konios, M. M. Stylianakis, E. Stratakis, E. Kymakis, *Journal of Colloid And Interface Science*, 2014, **430**, 108
- ²⁸ J. Liu, Y. Xue, Y. Gao, D. Yu, M. Durstock, L. Dai, *Adv. Mater.* 2012, **24**, 2228-2233.
- ²⁹ H. L. Poh, F. Sanek, A. Ambrosi, G. Zhao, Z. Sofer, M. Pumera, *Nanoscale*, 2012, **4**, 3515.
- ³⁰ W. S. Hummers, R. E. Offeman, *J. Am. Chem. Soc.*, 1958, **80**, 1339
- ³¹ D. Konios, C. Petridis, G. Kakavelakis, M. Sygletou, K. Savva, E. Stratakis, E. Kymakis, *Adv. Funct. Mater.*, 2015, **25**, 12213.
- ³² J.-Y. Kim, W. H. Lee, J. W. Suk, J. R. Potts, H. Chou, I. N. Kholmanov, R. D. Piner, J. Lee, D. Akinwande, R. S. Ruoff, *Adv. Mater.*, 2013, **16**, 2308
- ³³ K. C. Kwon, K. S. Choi, Y. Kim, *Adv. Funct. Mater.*, 2012, **22**, 4724
- ³⁴ L. Huang, Y. Liu, L.-C. Ji, Y.-Q. Xie, T. Wang, W.-Z. Shi, *Carbon*, 2011, **49**, 2431-2436.
- ³⁵ N. D. Lang, *Phys. Rev. B*, 1971, **4**, 4234
- ³⁶ B. P. Rand, D. P. Burk, S. R. Forrest, *Phys. Rev. B*, 2007, **75**, 115327
- ³⁷ L.-M. Chen, Z. Xu, Z. Hong, Y. Yang, *J. Mater. Chem.*, 2010, **20**, 2575-2598
- ³⁸ K. X. Steirer, P. F. Ndione, N. E. Widjonarko, M. T. Lloyd, J. Meyer, E. L. Ratcliff, A. Kahn, N. R. Armstrong, C. J. Curtis, D. S. Ginley, J. J. Berry, D. C. Olson, *Adv. Energy Mater.*, 2011, **1**, 813-820
- ³⁹ V. Shrotriya, G. Li, Y. Yao, C.-W. Chu, Y. Yang, *Appl. Phys. Lett.*, 2006, **88**, 073508
- ⁴⁰ B. R. Lee, J.-W. Kim, D. Kang, D. W. Lee, S.-J. Ko, H. J. Lee, C.-L. Lee, J. Y. Kim, H. S. Shin, M. H. Song, *ACS Nano*, 2012, **6**, 2984-2991
- ⁴¹ I. Riedel, J. Parisi, V. Dyakonov, L. Lutsen, D. Vanderzande, C. Hummelen, *Adv. Funct. Mater.*, 2004, **14**, 38
- ⁴² G. F. Burkhard, E. T. Hoke, M. D. McGehee, *Adv. Mater.*, 2010, **22**, 3293
- ⁴³ X. Li, X. Ren, F. Xie, Y. Zhang, T. Xu, B. Wei, W. C. H. Choy, *Appl. Opt. Mater.*, 2015, **3**, 1220

⁴⁴ D. H. Wang, J. K. Kim, J. H. Seo, I. Park, B. H. Hong, J. H. Park, A. J. Heeger, *Angew. Chem. Int. Ed.* 2013, **52**, 2874-2880

⁴⁵ P. Peumans, A. Yakimov, S. R. Forrest, *J. Appl. Phys.* 2003, **93**, 3693

⁴⁶ L. H. Slooff, S. C. Veenstra, J. M. Kroon, D.J.D. Moet, J. Sweelssen, M.M. Koetse, *Appl. Phys. Lett.*, 2007, **90**, 1435061